PLOS Biology

RESEARCH ARTICLE

Electrical Spinal Imaging: A noninvasive, high-resolution approach that enables electrophysiological mapping of the human spinal cord

Giulio Gabrieli[1,2], Richard Somervail[1,3], André Mouraux[4], Massimo Leandri[5], Patrick Haggard[6], Gian Domenico Iannetti[1,6]*

1 Neuroscience and Behaviour Laboratory, Italian Institute of Technology, Rome, Italy, **2** Digital Futures Research Hub, Technological University Dublin, Dublin, Ireland, **3** Translational and Computational Neuroscience Unit, Manchester Metropolitan University, Manchester, United Kingdom, **4** Institute of Neuroscience, Université Catholique de Louvain, Brussels, Belgium, **5** DINOGMI, Laboratory of Clinical and Experimental Electrophysiology, University of Genova, Genova, Italy, **6** Department of Neuroscience, Physiology and Pharmacology, University College London, London, United Kingdom

* g.iannetti@ucl.ac.uk, giandomenico.iannetti@iit.it

Check for updates

OPEN ACCESS

Citation: Gabrieli G, Somervail R, Mouraux A, Leandri M, Haggard P, Iannetti GD (2025) Electrical Spinal Imaging: A noninvasive, high-resolution approach that enables electrophysiological mapping of the human spinal cord. PLoS Biol 23(11): e3003116. https://doi.org/10.1371/journal.pbio.3003116

Academic Editor: Simon Hanslmayr, University of Glasgow, UNITED KINGDOM OF GREAT BRITAIN AND NORTHERN IRELAND

Received: March 8, 2025

Accepted: November 17, 2025

Published: November 26, 2025

Copyright: © 2025 Gabrieli et al. This is an open access article distributed under the terms of the Creative Commons Attribution License, which permits unrestricted use, distribution, and reproduction in any medium, provided the original author and source are credited.

Data availability statement: Raw data files are available at the Open Science Framework (https://doi.org/10.17605/OSF.IO/KHJCG).

Funding: This work was funded by the European Research Council (https://erc.europa.eu;

Abstract

The spinal cord is the key bridge between the brain and the body. However, scientific understanding of spinal cord function has historically been limited because noninvasive measures of its neural activity have proven exceptionally challenging. In this work, we describe an enhanced recording and analysis approach, Electrical Spinal Imaging (ESI), to obtain noninvasive, high-resolution images of the electrical activity of the human spinal cord. ESI is analytically simple, easy to implement, and data-driven: it does not involve template-based strategies prone to produce spurious signals. Using this approach, we provide a detailed description and physiological characterization of the spatiotemporal dynamics of the peripheral, spinal, and cortical activity elicited by somatosensory stimulation. We also demonstrate that attention modulates postsynaptic activity at spinal cord level. Our method has enabled five important insights regarding spinal cord activity. (1) We identified three distinct responses in the time domain: sP9, sN13, and sP22. (2) The sP9 is a traveling wave reflecting the afferent volley entering the spinal cord through the dorsal root. (3) In contrast, the sN13 and sP22 reflect segmental postsynaptic activity. (4) While the sP9 response is first seen on the dorsal electrodes ipsilateral to the stimulated side, the sN13 and sP22 were not lateralized with respect to the side of stimulation. (5) Unimodal attention strongly modulates the amplitude of the sP22, but not that of the sP9 and sN13 components. The proposed method offers critical insights into the spatiotemporal dynamics of somatosensory processing within the spinal cord, paving the way for precise noninvasive functional monitoring of the spinal cord in basic and clinical neurophysiology.

Consolidator Grant PAINSTRAT 649020 to GDI, and Proof of Concept Grant SPINREC 899963 to GDI). This work has been carried out within the Brain and Machines Flagship initiative of the Italian Institute of Technology. The funders played no role in the study design, data collection and analysis, decision to publish, and preparation of the manuscript.

Competing interests: The authors have declared no competing interests.

Abbreviations: BOLD, blood-oxygen level-dependent; CCA, canonical correlation analysis; CMS, Common Mode Sense; ESI, Electrical Spinal Imaging.

Introduction

Electrical brain potentials elicited by somatosensory stimulation are widely employed in basic research and clinical practice. They are routinely used to verify the functional integrity of afferent pathways [1], and have allowed obtaining a wealth of information about the spatiotemporal dynamics of the cortical processing of somatosensory input [2].

A similarly reliable, direct, and noninvasive readout of neural activity in the spinal cord in vivo would be equally informative, and has therefore been considered a key aim in sensory physiology [3]. Recent advances in fMRI technology have allowed recording blood-oxygen level-dependent (BOLD) signals arising in the spinal cord. However, in addition to the severe technical challenges posed by cardiac and respiration-induced movement artifacts, differences in magnetic susceptibilities of nearby tissues, cerebrospinal fluid inflow artifacts [4–6], the most important pitfall is the fact that BOLD signal integrates neural activities over several seconds, thus intrinsically limiting the ability to resolve neural events in time [7]. Thus, despite allowing localization of spinal responses during motor or somatosensory tasks [4,6,8], there has been a continuous effort to combine fMRI-based investigations with a more direct readout of the spinal electrical activity.

Recording the electrical activity of the spinal cord noninvasively is, however, not an easy task either. The first issue is neurophysiological: it is unclear whether the degree of regular arrangement of spinal neurons allows a reliable summation of postsynaptic potentials [9]. Indeed, while the scalp EEG results from the summation of synchronous activity from thousands of spatially-aligned cortical neurons [10], neurons within the cord are neither as numerous nor as aligned [9]. Second, surface recordings from the neck or dorsum skin are severely affected by muscular artifacts orders of magnitude larger than any neural signal. Third, cardiac activity similarly generates a massive artifact that, however, has the advantage of being predictable. Finally, the electrical activity of the somatosensory volleys ascending in the dorsal roots and intrinsic spinal tracts overlaps in space and time with the postsynaptic activity of the cord. All these factors result in an extremely low signal-to-noise ratio, unless epidural or intraparenchymal recordings are performed [11].

For this reason, recent attempts at recording the electrospinal activity have resorted to the use of selective spatiotemporal filtering and template-matching strategies to enhance the signal-to-noise ratio, such as denoising separation of sources [12] or canonical correlation analysis (CCA) [13]. These approaches are, however, computationally more resource-demanding, biased, and prone to the risk of creating spurious responses [14–17].

In this work, we propose a novel methodology, Electrical Spinal Imaging (ESI), that couples (1) high-density (63-channel) recording of the electrospinal activity with (2) a simple objective analysis pipeline based on conservative signal cleaning that minimizes the alterations of the spatiotemporal properties of the signal and does not rely on subjective operator-based decisions (Fig 1).

Using this approach, we provide a novel physiological characterization of the spatiotemporal dynamics of the peripheral, spinal, and cortical activity elicited by

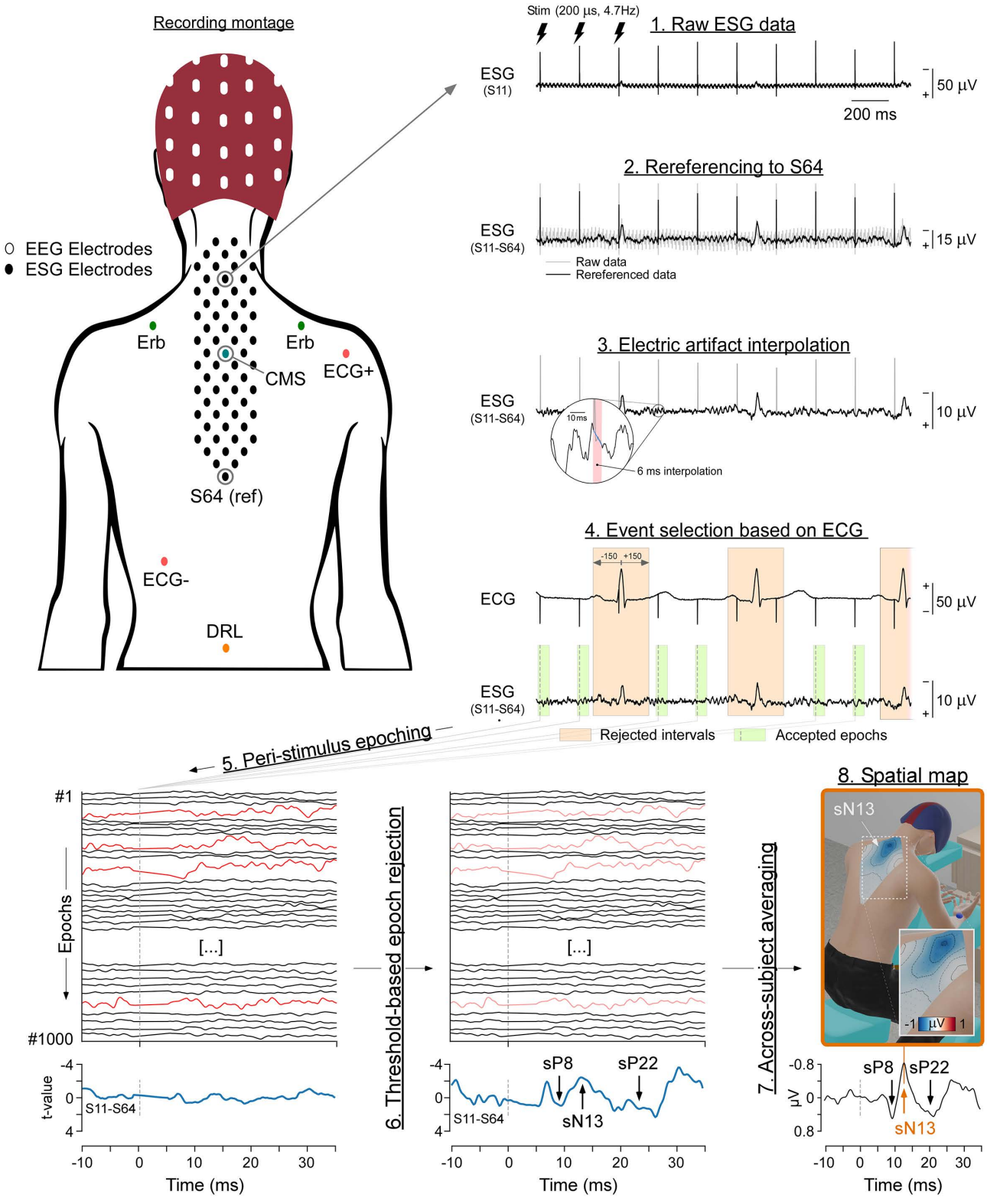

Fig 1. Recording setup and data analysis. *Top left panel:* Schematic of the position of the electrodes to record EEG (white), ESI (black), ECG (red), somatosensory activity at Erb's points (green), and the positions of Common Mode Sense (CMS, blue) and Driven Right Leg (DRL, orange) electrodes.

Note that Erb and ECG electrodes were placed on the chest, while ESI electrodes were placed on the back. *Top right and bottom panels*: Flowchart describing the analysis procedure. (1 and 2) Raw ESI signals are first re-referenced to the most caudal dorsal electrode (S64). (3) The artifact caused by the electrical stimulation of the median nerve is removed by linear interpolation. (4) The ECG is used to identify ESI time windows contaminated by the QRS complex (orange). This allows subsequent selection of ESI time windows to retain. (5) These time windows are epoched around the somatosensory stimulus. (6) An amplitude-based threshold is used to identify and remove artifactual epochs (red). (7) Resulting artifact-free epochs are averaged across stimuli of each block. Subject-level average waveforms are subsequently averaged across participants. (8) Images of the spatial distribution of spinal cord activity are calculated by spline interpolation across ESI electrodes. The figurine depicts spinal cord activity at the latency of the N13 wave.

https://doi.org/10.1371/journal.pbio.3003116.g001

somatosensory stimulation. We demonstrate a specific circuit mediating the attentional modulation of postsynaptic activity at spinal cord level.

Methods

Participants

Thirteen healthy human participants (mean ± SD age 28.8 ± 5.6 years, range 19–37 years, 7 females) gave written informed consent before taking part in the study. Procedures were approved by the ethical committee of the Fondazione Santa Lucia, Rome, Italy (number CE/788). The study was conducted according to the principles expressed in the Declaration of Helsinki.

Experimental design

Experiments took place in a dim, quiet, temperature-controlled room. Participants were seated in a massage chair with their neck supported in a flexed position via a face cradle, and their arms kept semi-flexed and resting on two dedicated supports. Participants were asked to keep their gaze stable and minimize spontaneous eye blinks.

The experiment consisted of 8 successive blocks, each lasting approximately 4 min. Each block consisted of 1,000 somatosensory stimuli delivered at 4.75 Hz. The interval between consecutive blocks was approximately 2 min. In 4 blocks, stimuli were delivered to the left median nerve. In the other 4 blocks, stimuli were delivered to the right median nerve. The stimulated side was alternated in each block. In half of the participants, the first block entailed the stimulation of the right median nerve.

In each block, the stream of somatosensory stimuli was interrupted by a few omissions of individual stimuli. Omissions were randomly distributed across the block, subject to the constraint that at least 5 consecutive stimuli had to be delivered between omissions. The number of omissions ranged from 2 to 25 per block, with a rectangular distribution. With the standard interstimulus interval being 211 ms, the interval between two stimuli separated by an omission was 420 ms. Before each block, participants were instructed to either (1) count the number of omissions (*omission counting*), or (2) memorize a sequence of eight capital letters presented on an A4 page for a maximum of 2 min prior to starting the block (*letter memorization*). At the end of each block, participants were required to report either the number of omissions or the sequence of letters. There were 2 omissions counting and 2 letter memorization blocks per stimulation side. In half of the participants, the first block entailed the omission counting task. Each experimental session lasted approximately 3 hours, about half of which was devoted to the positioning of the recording and stimulating electrodes.

Sensory stimuli

Somatosensory stimuli were constant-current, biphasic square-wave electrical pulses (200 μs duration; DS8R, Digitimer, UK) delivered using a surface bipolar electrode (0.5 cm diameter, 3 cm interelectrode distance, cathode sited proximally) placed over the median nerve of either the left or the right wrist. The intensity of somatosensory stimulation was initially adjusted for each participant to elicit a reproducible thumb muscle twitch, and during the stimulation blocks it was set 10% above this motor threshold, thus delivering a mixed sensorimotor stimulus.

Spinal recording

The electrical activity of the spinal cord was recorded using 63 active electrodes placed on the skin of the back (dorsal electrodes; Fig 1). Electrodes were arranged in 7 rostrocaudal columns: 1 column aligned on the spinal midline, and 6 parasagittal columns (3 to the right and 3 to the left side of the midline). The distance between adjacent columns was 7.5 mm. From left to right, the number of electrodes composing the seven columns was: 8, 9, 10, 9, 10, 9, 8. The center-to-center distance between consecutive electrodes within each column was 3 cm. The two most rostral electrodes, which belonged to columns 3 and 5, were placed at the level of C2, each 7.5 mm from the midline (Fig 1). The remaining electrodes were progressively placed according to the above interelectrode distances. Thus, the entire array covered the skin spanning from the 2nd cervical (C2) to approximately the 8th thoracic (T8) vertebra. Two additional electrodes were placed on the left and right Erb's points, to record the activity from the brachial plexus. The Common Mode Sense (CMS) and Driven Right Leg (DRL) electrodes were placed on the midline, one at the center of the array and the other at the level of the 3rd lumbar vertebra (L3), respectively.

Signals were amplified and digitized at a sampling rate of 4,096 Hz (Biosemi Active-2 system). The same amplifier was used to simultaneously record the EEG and the ECG (see section "EEG and ECG recordings"). Biosemi active electrode offsets were kept below 20 mV.

EEG and ECG recordings

The EEG was recorded using 32 active electrodes placed on the scalp according to the International 10–20 system. The ECG was recorded using two surface electrodes placed on the anterior aspect of the right shoulder and at the level of the seventh intercostal space on the left mid-clavicular line.

Data processing

All electrophysiological data were preprocessed and analyzed in Python (3.10.12) using the *mne* [18], *numpy* [19], and *scipy* [20] packages. ECG analysis, filtering, and resampling of the data used the default *mne* implementation, unless differently specified.

ECG processing. Continuous ECG signals were first band-pass filtered at 5–35 Hz (zero-double phase FIR filter with a Hanning window of 10 s, as implemented in *mne*). Then, the latency of the R peak of each QRS complex was identified using a validated method implemented in *mne* [18]. This procedure allowed removal of stimulation epochs from both electrocortical and electrospinal data that occurred within ±150 ms of the R peak, as described below.

ESI and EEG processing. A series of preprocessing steps was adopted to yield ESI and EEG epochs free from the large artifacts consequent to (1) electrical stimulation, (2) heartbeat, (3) muscular activity, and (4) other sources of noise. The overall ESI procedure is depicted in Fig 1.

Continuous ESI and EEG data were first re-referenced to the most caudal spinal electrode (S64; Fig 1), and to Fz, respectively. Then, electrical stimulation artifacts were removed by linearly interpolating the signal from 1 ms before to 5 ms after the onset of each stimulus. At this point, both ESI and EEG data were band-pass filtered (50–800 Hz, zero-phase FIR filter with a Hamming window of 1,083 samples (264 ms), as implemented in *mne*). Dorsal electrodes with signal amplitude with a variance >5 times larger than the variance of the mean across channels for at least 50% of the stimulation periods were removed and spline interpolated using the neighboring electrodes. Across participants, the mean number of interpolated electrodes was 10.3 ± 3.7% of the total number of electrodes.

In the resulting continuous data, somatosensory stimuli that occurred within ±150 ms from the R peak were excluded from the subsequent analysis. These discarded stimuli constituted 33.9 ± 14.9% (range 21.7%–45.8%) of the total number of stimuli per subject. The proportion of stimuli discarded depended largely on the participant's heart rate. We note that discarding ~34% of trials to reject cardiac artifacts and optimize signal-to-noise ratio is not data efficient, especially

in clinical populations or less controlled environments. To address this limitation, some authors have adopted a different strategy: pacing the stimulation to the cardiac cycle and thereby delivering somatosensory stimuli only in the silent phases between two consecutive QRS complexes [e.g., 21–23]. This strategy, however, requires a stimulation system based on a real-time ECG analysis, and does not improve the overall ratio between acquisition time and number of artifact-free trials.

The remaining continuous data were thereupon segmented into 300-ms long epochs (−100 to +200 ms) relative to the onset of the stimuli. These epochs were baseline corrected using the −100 to −1 ms interval as a reference, and linearly detrended.

Finally, epochs with peak-to-peak amplitude values exceeding a threshold between 100 and 250 μV (160 ± 44 μV; defined individually according to the signal-to-noise ratio) in at least one electrode (i.e., epochs probably contaminated by artifacts) were rejected. Considering both ESI and EEG datasets, these epochs were 2.2% ± 2.9% of the total number of epochs devoid of ECG artifacts.

The resulting clean epochs were labeled according to the possible combinations of the four experimental conditions (stimulation side: right or left; cognitive task: omission counting, letter memorization).

To investigate the differences in the responses elicited by right and left median nerve stimulation, all epochs obtained during the omission and letter memorization tasks were pooled. This procedure yielded two average waveforms per participant (right and left stimulation). In contrast, to investigate the differences in the responses elicited during the omission versus letter memorization task, all epochs obtained following right median nerve stimulation were flipped with respect to the midline, so that they could be pooled with the data obtained following left median nerve stimulation. This procedure yielded two additional average waveforms per participant (omission and letter memorization). Finally, to investigate the temporal and spatial properties of the response along the somatosensory pathways, the flipped epochs were pooled across tasks, as if the stimuli were always delivered to the left side. This procedure yielded one additional average waveform per participant.

Given that early-latency somatosensory responses are notoriously variable across individuals as a function of arm length and height [24], to minimize interindividual variability and perform group-level statistics, single-subject average waveforms were peak aligned using a validated procedure based on linear time-warping [25,26]. Specifically, we aligned (1) eN9 peaks measured at the ipsilateral Erb's point, (2) sN13 peaks measured at midline dorsal electrode S8, and (3) cN20 and cP25 peaks measured at the contralateral parietal scalp electrode Pc.

After realignment, the single-subject average waveforms were averaged to obtain group-level waveforms. Group-level topographies were computed by spline interpolation. In this work, we did not perform time-frequency analysis of the EGI time series as our primary goal was to identify time-domain components related to transient somatosensory stimulation. Nevertheless, time-frequency approaches may be more suitable for detecting longer-lasting spinal activities, such as those arising from the activation of corticospinal pathways during voluntary movements.

Latency maps

To determine whether the recorded components, such as the sP9 and sN13, reflect traveling far-field action potentials or local postsynaptic activity, we computed spatial maps of peak latency distributions of signals [27]. For visualization purposes, signals were upsampled 10-fold using FFT-based resampling (window size 200 ms). This method preserves the spectral properties of the original signal while providing an effectively denser temporal sampling. We restricted this analysis to the electrodes positioned in the top 8 rows of the spinal recording array above the CMS electrode, where the sP9 and sN13 components occur (Fig 1, top left panel and Fig 2). We measured, separately for each component, the peak latency from each electrode, and we subsequently color-coded peak latency relative to the electrode with the shortest latency (Fig 4). In these images, traveling action potentials would appear as a smooth and continuous unidirectional gradient. On the contrary, the lack of such a unidirectional gradient would suggest that the component observed in the time domain reflects local postsynaptic activity.

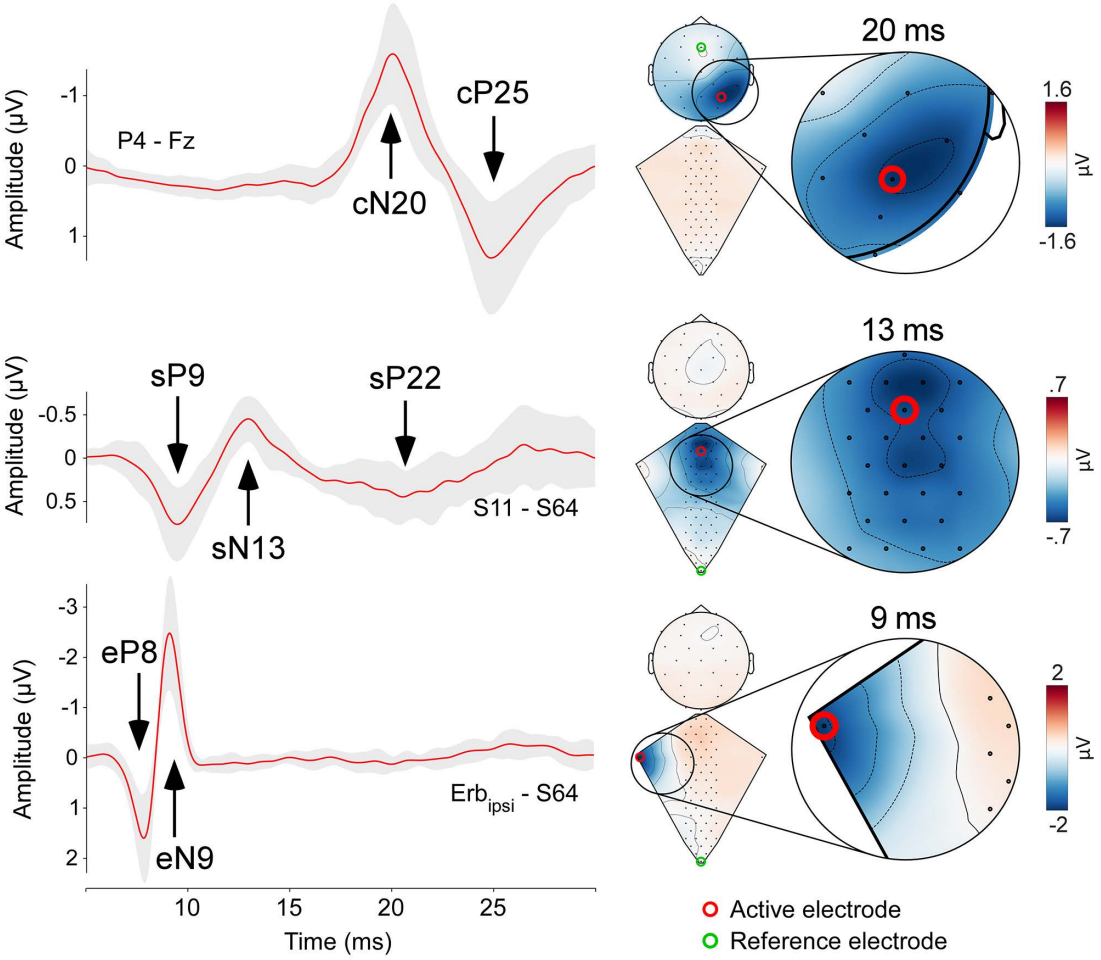

Fig 2. Neural activity along the somatosensory pathways in response to transcutaneous electrical stimulation of the median nerve at the wrist. Responses recorded from the ipsilateral brachial plexus (eP8 and eN9, bottom row), the spinal cord (sP9, sN13, and sP22, middle row), and the cerebral cortex (cN20-cP25, top row). Left column: red waveforms are group-level averages, while the gray shade represents the standard deviation (±1 standard deviation). Right columns: dorsum and scalp maps obtained using cubic interpolation of multielectrode recordings (dorsum: 63 electrodes; scalp: 32 electrodes). Maps are shown at the latency of the eN9, sN13, and cN20 peaks. Red circles show the electrodes from which waveforms shown in the left column are extracted. Green circles show the reference electrode for both waveforms and maps: dorsal recordings are referenced to the most caudal electrode (S64), whereas scalp recordings are referenced to Fz. Enlargements show areas of maximal response amplitude. The data underlying this figure can be found at https://doi.org/10.17605/OSF.IO/KHJCG.

https://doi.org/10.1371/journal.pbio.3003116.g002

Lateralization analysis

To determine whether the EEG and ESI responses were lateralized as a function of the stimulated side, single-subject waveforms elicited by right and left median nerve stimulation were compared using a point-by-point paired sample *t* test using a 3-fold cross-validation. The significance level was set at $p = 0.01$. To correct for multiple comparisons, an electrode was considered significant only if (1) it was part of a cluster of at least three adjacent electrodes with a *p*-value < 0.01, and (2) it was part of a time window with an average $p < 0.01$ in at least 4 consecutive time points (i.e., for a duration of at least 1 ms). Group-level difference waveforms (left *minus* right) were calculated to show their spatial distribution. Dorsal and scalp topographies and their differences were plotted at the peak latency of the eN9, sN13, cN20, sP22, and cP25 waves.

Attentional task analysis

To determine whether the EEG and ESI responses were different as a function of the attentional task, we performed the same procedure described above but compared the omission counting and letter memorization conditions. Group-level difference waveforms were calculated as letter memorization *minus* omission counting (Fig 6).

Results

Response waveforms and topographies

At single-subject and group-level, somatosensory stimuli elicited clear responses from the brachial plexus (eP8 and eN9), the spinal cord (sP9, sN13, sP22), and the brain (cN20 and cP25, Fig 1, left panel). By exploiting a high-density spatial sampling, we were able to reveal how the neural activity along the somatosensory pathways unfolds in time and space with sub-millisecond temporal resolution (Fig 2 and S1 and S2 Videos).

Erb components. We were able to identify the traveling afferent volley at the brachial plexus ipsilateral to the stimulated side, in the form of a positive-negative complex (eP8/eN9). Its average amplitude and duration (calculated, at Erb, spinal, and scalp recordings, as the width at half maximum) were as follows: eP8 2.0 ± 0.9 μV, 1.9 ± 0.5 ms; eN9 −2.9 ± 1.0 μV, 1.8 ± 0.2 ms.

Spinal components. Concomitant with the eN9 wave at the brachial plexus, upper dorsal electrodes disclosed a first positive spinal response peaking around 9.5 ms post-stimulus (sP9: 0.93 ± 0.3 μV, 3.2 ± 0.8 ms; channel S8), followed by the sN13 wave (−0.9 ± 0.4 μV, 3.7 ± 0.8 ms; channel S8). Both sP9 and sN13 had a single clear maximum, centered on the dorsal electrodes overlying the spinal segments C4 to C6, with no clear lateralization (Figs 2 and 3). After the end of the sN13 wave, there was a period of ~3 ms with no sign of electrical activity, interrupted by the occurrence of a longer-lasting positive wave (sP22: 0.7 ± 0.4 μV, 5.5 ± 1.7 ms; channel S8). sP22 had a maximum over the midline dorsal electrodes overlying the spinal segments C4 to C7. Compared to the earlier spinal responses (sP8 and sN13), sP22 was longer-lasting and more widespread in both the rostrocaudal and the mediolateral directions (Figs 2 and 3), suggesting a longer-loop, more polysynaptic generation mechanism compared to the earlier, sharper spinal components.

Scalp components. At scalp level, somatosensory stimuli elicited the canonical cN20-cP25 complex, maximal over P3/4 CP5/6 and P7/8, i.e., the electrodes broadly corresponding to the hand representation of the primary somatosensory cortex contralateral to the stimulated side [28] (Fig 2). The amplitude and duration of the cN20-cP25 complex were as follows: cN20: −2.1 ± 0.9 μV, 5.4 ± 0.7 ms; cP25: 1.6 ± 1.0 μV, 6.5 ± 1.4 ms.

Temporal dynamics of spinal responses

To gain insight into the nature of the sP9 and sN13 components, and specifically to understand whether they represent far-field traveling action potentials or segmental postsynaptic activity, we built latency delay images, where colors indicate the peak latency delay relative to the electrode with the shortest latency (Fig 4). For the sP9 wave, latency delays followed a clear gradient, whose spatial distribution indicated that the sP9 reflects far-field action potentials entering the spinal cord at ~C6-C7 level, and traveling in the lateral-medial and caudal-rostral directions (Fig 4, top). S3 Video shows the sP9 sweeping the field of view from the ~C6-C7 entry level to the most rostral dorsal electrodes. In contrast, the sN13 did not show signs of traveling (Fig 4, bottom).

Taken together, these results suggest that the sP9 mostly reflects the extracellular events associated with the propagation of action potentials of Aß afferent fibers entering the spinal cord from the brachial plexus and the dorsal roots, and then traveling in the dorsal columns. In contrast, sN13 seems to largely reflect postsynaptic activity occurring in the dorsal horn at C4-C6 levels, consequent to the arrival of the Aß afferent input.

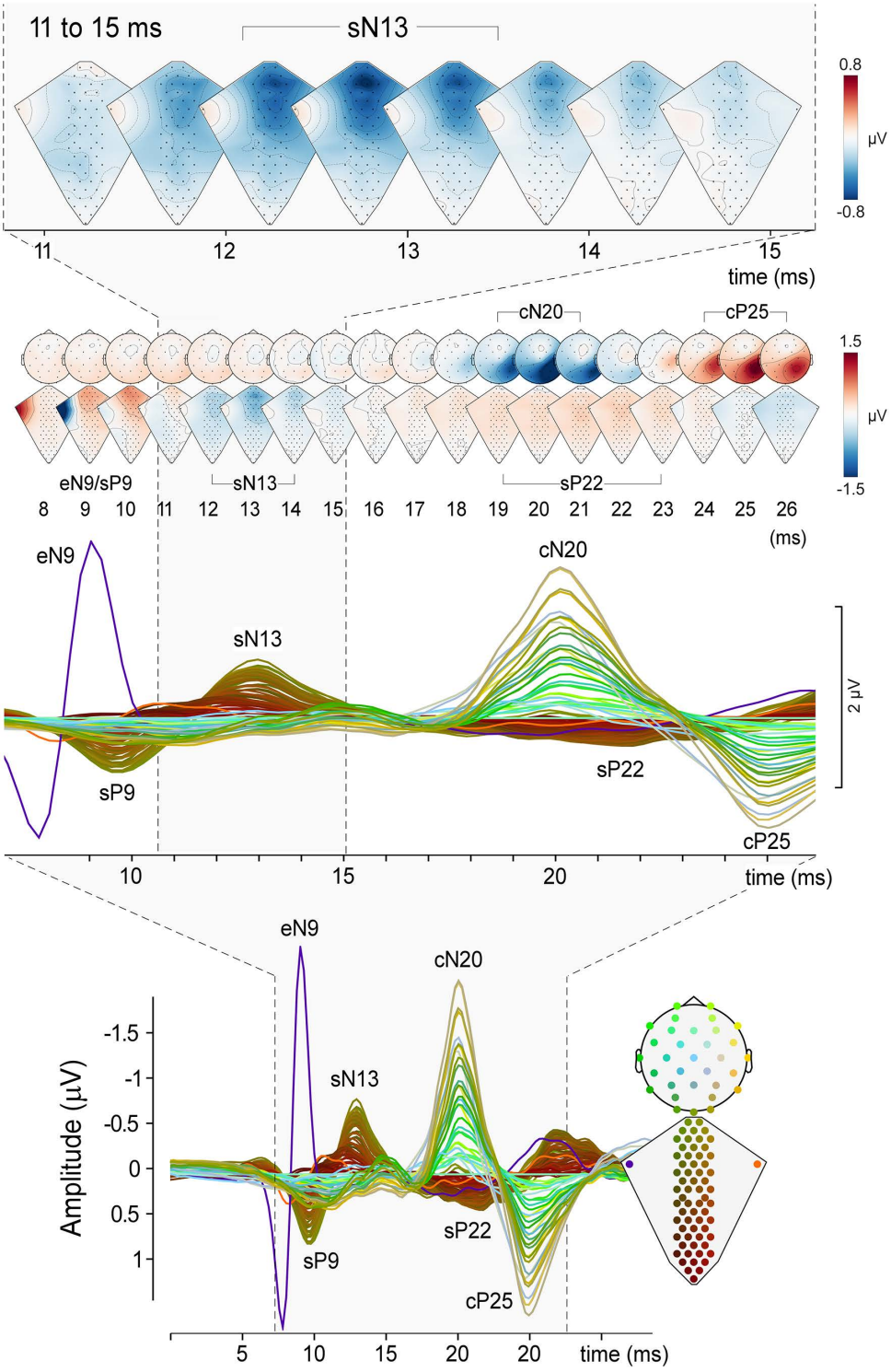

Fig 3. Electoral Spinal Imaging (ESI): High-resolution images of spinal cord activity during somatosensory stimulation. *Bottom panel*: Recordings obtained using 97 electrodes (2 electrodes located on the right and left ERB points, 63 dorsal electrodes spanning from the cervical (C2) to the thoracic (T8) segments, and 32 scalp electrodes). The electrode positions shown in the bottom right figurine and their recording of the response elicited by somatosensory stimulation (right) are color-coded such that neighboring channels have similar colors. Signals were referenced as described in Fig 1. *Middle panel*: Enlargement of the responses between 8 and 26 ms poststimulus. *Top panel*: Lower row shows dorsal and scalp maps with 1-ms

resolution. The eN9, sP9, sN13, sP22, cN20 and cP25 peaks are labeled. Upper row enlarges the dorsum maps of spinal cord activity between 11 and 16 ms poststimulus. Note the peak of postsynaptic activity occurring around 13 ms poststimulus. The data underlying this figure can be found at https://doi.org/10.17605/OSF.IO/KHJCG.

https://doi.org/10.1371/journal.pbio.3003116.g003

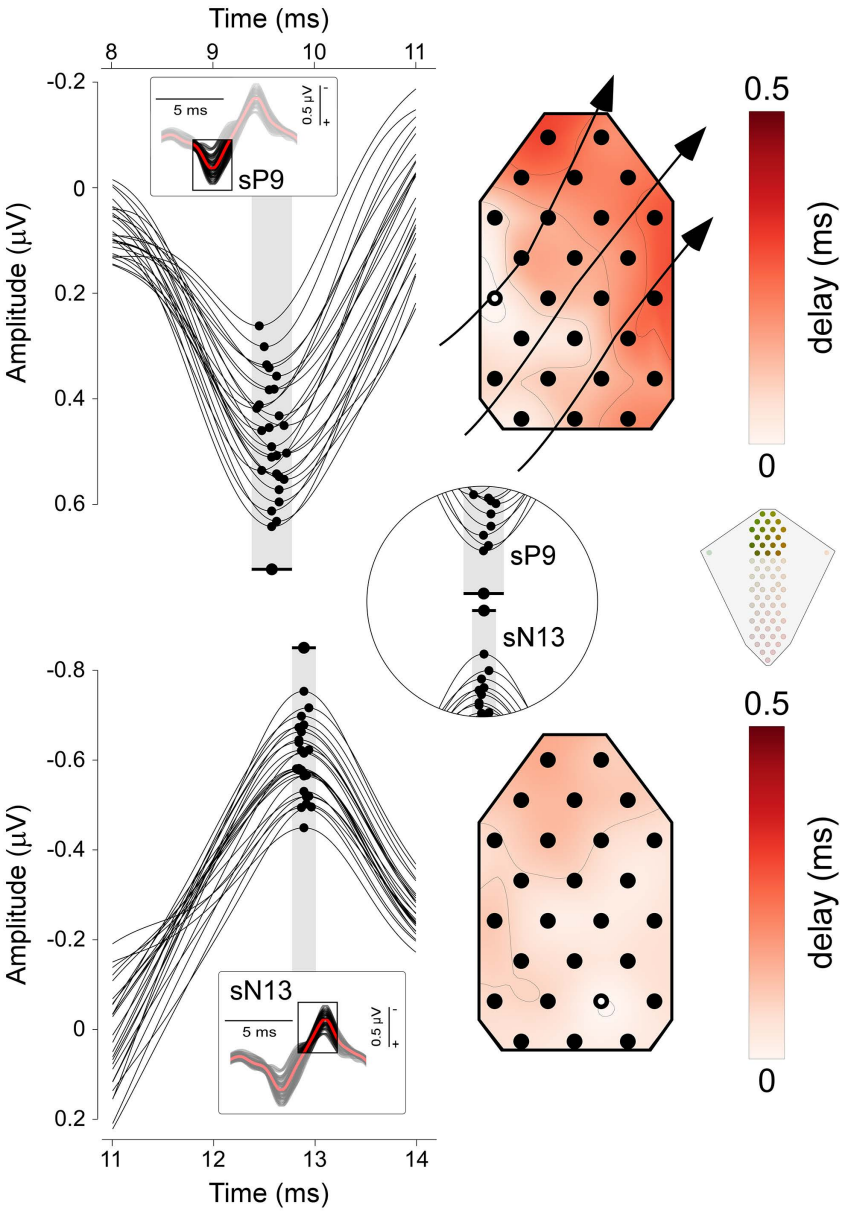

Fig 4. Latency distributions of the sP9 and sN13 waves. Group-level data. *Left column*: sP9 (top) and sN13 (bottom) waves recorded from the top dorsal electrodes. Insets show the response over a larger time window; the box indicates the intervals around sP9 and sN13. Dots indicate the peak latency recorded from each electrode. The black dot and the horizontal black bar indicate the mean latency and latency range, respectively. *Right column*: Maps of the latency delays, with color-coding of time relative to the electrode with the shortest latency (highlighted in white, used as time 0). Note how, for the sP9 wave, the electrodes with shortest (whiter regions of spinal electrode topography, broadly corresponding to the C6-C7 segment) and longest latencies (redder regions) show a clear spatial gradient, indicating that the sP9 wave travels in the lateral-medial and caudal-rostral directions. Compare with the lack of any clear spatial gradient in the sN13. See also S3 Video. The data underlying this figure can be found at https://doi.org/10.17605/OSF.IO/KHJCG.

https://doi.org/10.1371/journal.pbio.3003116.g004

Response lateralization

Fig 5 shows the grand average ESI and EEG waveforms superimposed, together with the dorsal and scalp topographies at the peak latency of the eN9, sN13, cN20, sP22, and cP25 waves, for each stimulation side. The topography of eN9 elicited by median nerve stimulation displayed a clear negative maximum at the electrode detecting the activity of the brachial plexus ipsilateral to the stimulated side. We observed a larger eN9 amplitude in the ERB_{ipsi} compared to the ERB_{contra} electrode ($p = 0.0008$, paired-sample t test). In contrast, the topography of the sN13 and sP22 waves was similar following right and left stimulation, with no electrodes showing significant differences (p-value range = 0.066–0.906).

At scalp level, the topographies of both the cN20 and cP25 waves were clearly lateralized. The cluster of electrodes overlying the primary somatosensory cortex contralateral to the stimulated side displayed higher amplitudes compared to the ipsilateral side (cN20: mean p-value = 0.004, p-value range = 0.0002–0.0096; cP25: mean p-value = 0.0011, p-value range = 1.5×10^{-7}–0.005; paired-sample t test).

Attentional modulation

Fig 6 shows, for each attentional condition, the grand average ESI and EEG waveforms superimposed, together with the dorsal and scalp topographies at the peak latency of the eN9, sN13, cN20, sP22, and cP25 waves. We found strong evidence for a larger sP22 amplitude in the letter memorization condition (mean p-value = 0.003, p-value range = 0.0001–0.0099; paired-sample t test). In contrast, the eN9 and sN13 amplitudes were similar during the two attentional tasks, with not enough electrodes showing significant differences (p-value range = 0.061–0.896). Similarly, there was no evidence of any difference in the amplitude of the cN20 and cP25 (cN20: p-value range = 0.0463–0.722; cP25: p-value range = 0.060–0.856; paired-sample t test).

Discussion

In this work, we describe a recording and analysis approach to obtain images of the electrical activity of the spinal cord non-invasively and with high temporal and spatial resolution (Electrical Spinal Imaging, ESI). Crucially, this approach does not entail any form of template-matching strategies (such as CCA; [13,15,17]), which are prone to generate the false belief of consistent responses [16].

Exploiting this ESI approach, we provide a detailed description and physiological characterization of the spatiotemporal dynamics of the peripheral, spinal, and cortical activity elicited by somatosensory stimulation. Importantly, we demonstrate how cognition can modulate postsynaptic activity at spinal cord level.

We obtained four key results regarding spinal cord activity: (1) We identified three distinct responses: sP9, sN13, and sP22. (2) The sP9 is a traveling wave, while the sN13 and sP22 reflect local, postsynaptic activity. (3) While the sP9 response is first seen on the dorsal electrodes ipsilateral to the stimulated side, the sN13 and sP22 were not clearly lateralized with respect to the side of stimulation. (4) Attention strongly modulates the amplitude of the sP22, but not that of the sP9 and sN13.

Bipolar shape of the eP8/eN9 complex: Comparison with the tripolar shape of near nerve recordings

With the electrodes located at the Erb point, we recorded the classical traveling afferent volley at the brachial plexus ipsilateral to the stimulated side as a positive-negative bipolar eP8/eN9 complex (Figs 2 and 3 and S1 and S2 Videos). This pattern contrasts with the classical descriptions of a triphasic positive-negative-positive pattern recorded when action potentials travel along nerve fibers [e.g., 29,30]. This difference may arise because classical monopolar extracellular nerve recordings use an active electrode detecting the depolarization occurring along the fiber: the active electrode sees first the approaching sink (first positivity), then the sink passes under the electrode (large negative deflection), and finally the sink goes away (second positivity) [30]. In contrast, our recordings showed a biphasic, not a triphasic pattern. This

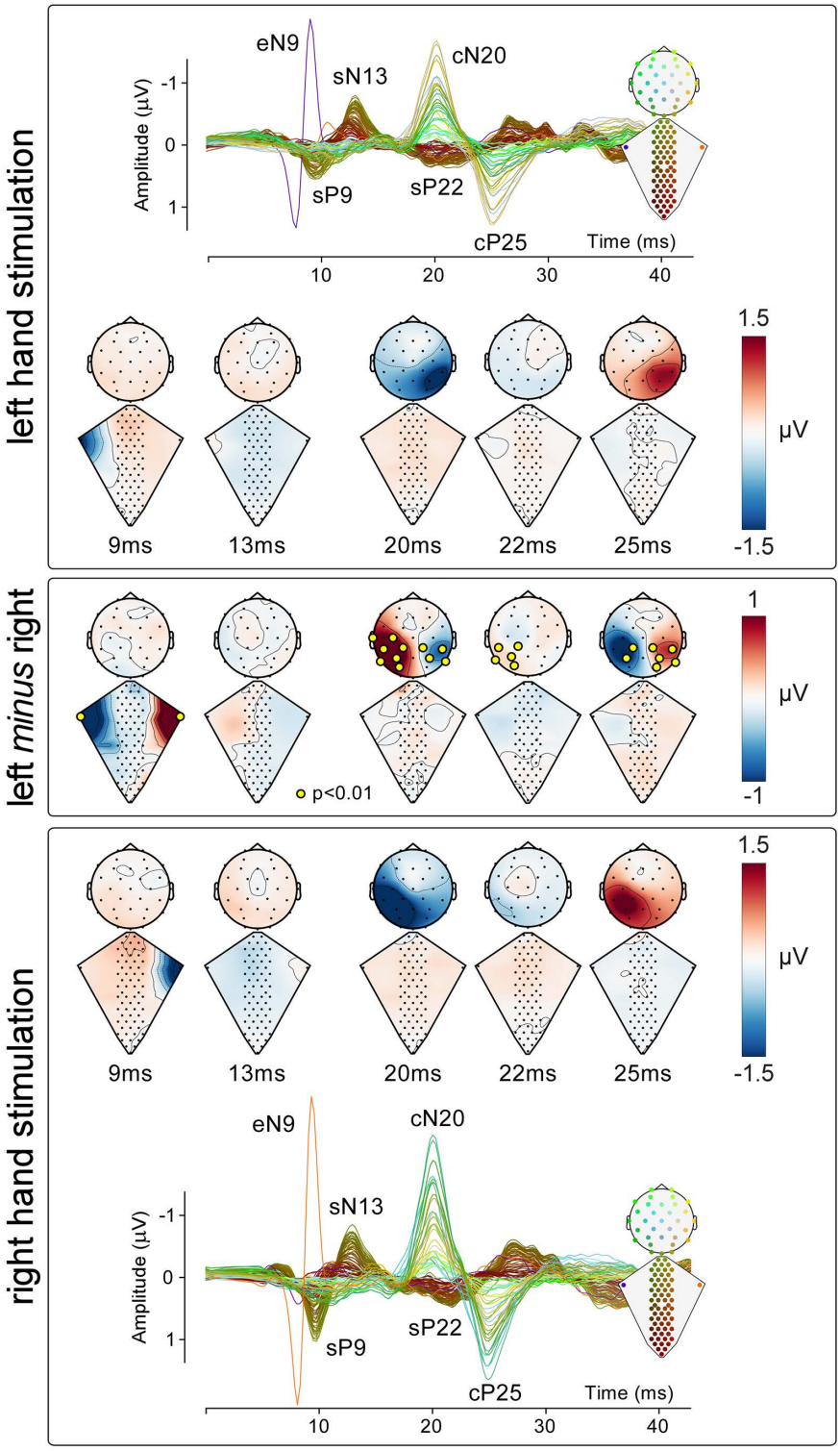

Fig 5. Lateralization of neural responses along the somatosensory pathways. *Top and bottom panels*: Neural responses recorded along the somatosensory pathways following the stimulation of the median nerve at the left and right wrist, respectively. Top and bottom panels display the group-level response superimposed from all 97 electrodes, referenced to S64 for the spinal electrodes, and to Fz for the scalp electrodes. Electrode position and responses are color-coded according to the scheme shown in the inset. These panels also contain dorsum and scalp maps at the latency of the

eN9, sN13, cN20, sP22, and cP25 peaks. Middle panel: Difference maps obtained by subtracting the right response from the left response, at the same latencies as the maps shown in the top and bottom panels. Yellow circles identify electrodes showing statistically significant effects ($p < 0.01$, cluster-corrected in both time and space; see Methods for details). Note the clear lateralization of the response recorded from the brachial plexus (eN9) and the brain (cN20 and cP25), and the lack of lateralization of the spinal responses (sN13 and sP22). The data underlying this figure can be found at https://doi.org/10.17605/OSF.IO/KHJCG.

https://doi.org/10.1371/journal.pbio.3003116.g005

biphasic pattern may reflect the so-called *end potential* phenomenon, in which the second positive component is attenuated because the "going away" phase escapes the detection field of the electrode, due to either a change of direction of the axon or to an end synapse [31].

We now discuss each of the three components that we identified in dorsal recordings (sP9, sN13, and sP22; Figs 1 and 2 and S1 and S2 Videos).

The sP9 reflects somatosensory input entering the cord through the dorsal roots

Invasive and noninvasive studies in a number of species, including rodents, human, and nonhuman primates, also described that the earliest spinal response following somatosensory stimulation is a positive deflection (labeled as P1 or P9) [32]. Invasive experiments using serial recordings at different locations along the cord convincingly identified the origin of this component in the afferent volley traveling through the dorsal roots into the spinal cord [33]. The high-spatial resolution of ESI allowed us to investigate this traveling property of the sP9 component directly. Our latency delay images confirmed that the sP9 wave first appears in the lateral electrodes ipsilateral to the stimulated side at C6-C7 level, and then travels along both lateral-medial and caudal-rostral directions (Fig 4 and S1 and S3 Video). Thus, the sP9 likely reflects the current sink entering the cord through the dorsal roots and traveling rostrally along the dorsal column tracts (Fig 7, S3 Video).

The sN13 reflects segmental postsynaptic activity in the dorsal horn

The sP9 was followed by the sN13 (Figs 2 and 3). In striking contrast with the sP9, the sN13 was stationary: while also appearing on the dorsal electrodes overlying the C6-C7 segments, it lacked the traveling-wave profile that characterized the sP9 (Fig 4 and S1, S2 and S3 Videos). Thus, the sN13 likely reflects postsynaptic activity occurring locally, at the level of the dorsal horn. Our sN13 is equivalent to the so-called N1 recorded both subdurally and intraparenchymally in cats, dogs, humans, and nonhuman primates [34–39]. The observations that the N1 is measured (1) already in response to low stimulus intensities activating large-diameter A-afferents [34], (2) maximally at the segmental level that corresponds to the stimulated dermatome [40], and (3) at the same segmental level as the traveling sP9, all indicate that the sN13 reflects the postsynaptic activity occurring in laminae IV and V. Thus, we take the sN13 observed in our recordings as a noninvasive readout of the postsynaptic activity occurring in the deep dorsal horn following the first arrival of somatosensory input (Fig 7). Given the sP9-sN13 latency and the average length between stimulation site and recording electrodes of ~70 cm, this input travels along medium-diameter type-II Aβ afferents conducting at approximately 50–70 m/s.

The sP22 reflects top-down supraspinal projections

The latest spinal component sP22 was also maximal on the electrodes overlying C4-C7 spinal segments. Compared to the preceding sP9 and sN13, it was longer-lasting and more widespread in both rostrocaudal and mediolateral directions (Figs 2 and 3).

In animal studies, the P1-N1 waves (corresponding to our sP9-sN13) are immediately followed by a lower-frequency positivity that is typically divided into two distinct components: a "fast" P2f and a "slow" P2s. The P2f, which is only observed in invasive recordings [41] and resists spinal transection [42], is interpreted as reflecting a primary afferents depolarization [43]. The subsequent P2s, in contrast, depends on the animal's behavioral state and is abolished by spinal transection, indicating that it reflects the consequences of top-down supraspinal projections [44,45].

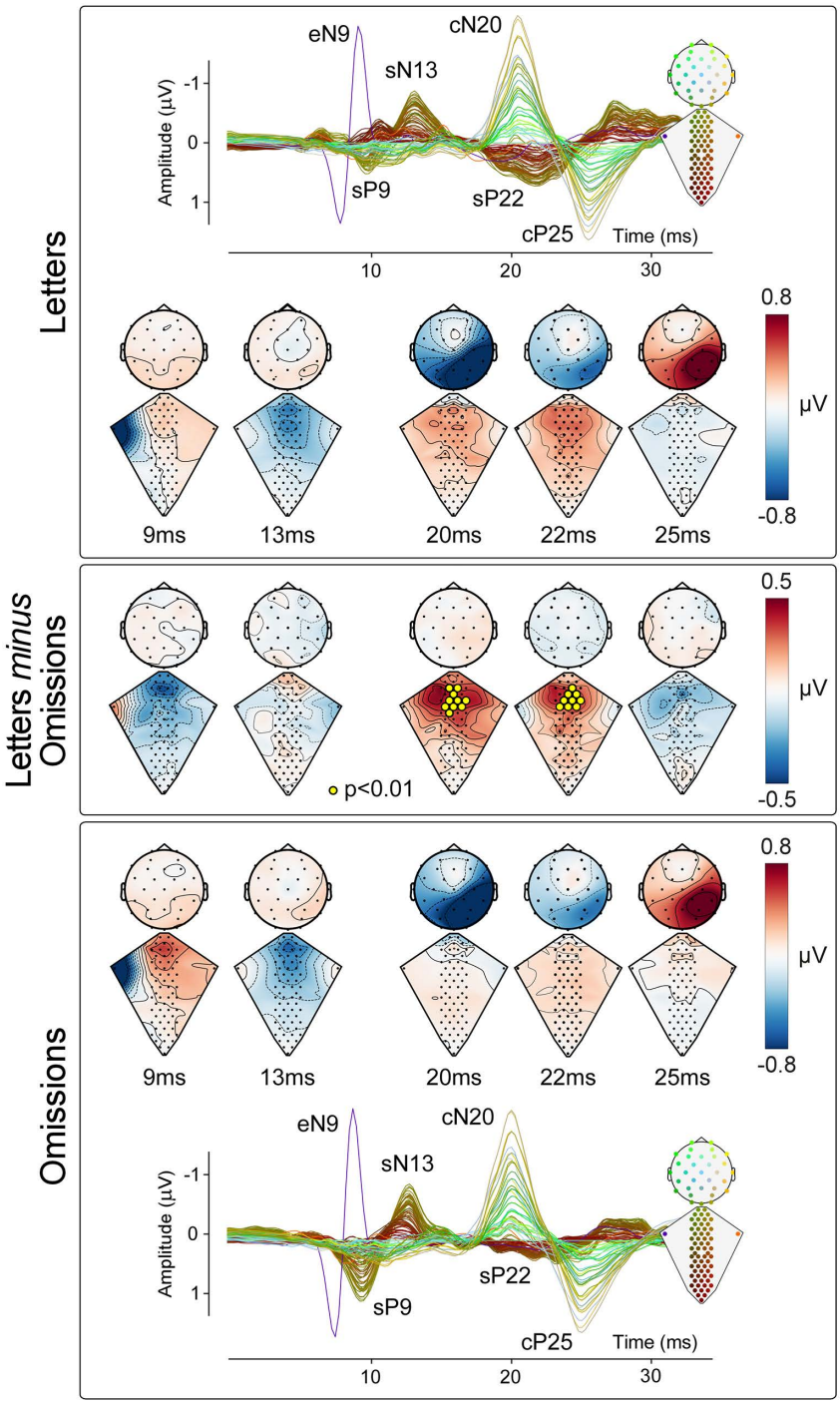

Fig 6. Attentional modulation of spinal cord activity. *Top and bottom panels*: Neural responses recorded along the somatosensory pathways under the conditions of letter memorization (top panel), and attention to somatosensory stimulation (counting omissions, bottom panel). Both panels show the group-level response distribution on the dorsum and scalp at the eN9, sN13, cN20, sP22, and cP25 peak latencies. Electrode position and responses are color-coded according to the scheme shown in the inset. *Middle panel*: Difference maps obtained by subtracting the responses elicited during the omission task from those elicited during the letter memorization task, at the same latencies as the maps in the top and bottom panels. Yellow circles identify electrodes showing statistically significant effects ($p < 0.01$, cluster-corrected in both time and space; see Methods for details). Note the significant difference in the cluster of spinal electrodes centered on the sP22, and the lack of differences in the early-latency cortical SEPs. The data underlying this figure can be found at https://doi.org/10.17605/OSF.IO/KHJCG.

https://doi.org/10.1371/journal.pbio.3003116.g006

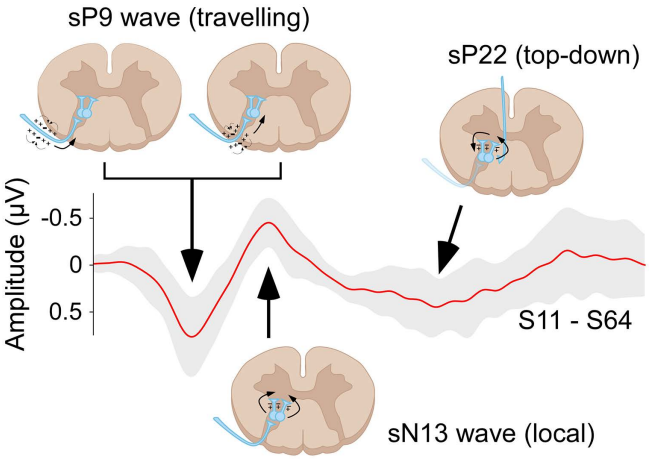

Fig 7. Neural generators of the recorded responses. Schematic representations of the putative spinal mechanisms generating the electrocortical responses recorded with ESI. The sP9 appears as a traveling wave (see also the delay map in Fig 4) as it reflects the current sink entering the cord through the dorsal roots and traveling rostrally along the dorsal column tracts. In contrast, the stationary sN13 reflects the segmental postsynaptic activity occurring in the deep dorsal horn following the first arrival of somatosensory input. Finally, the late sP22 is not directly consequent to a local, segmental effect of the incoming somatosensory input, but instead reflects stimulus-triggered activation of a long-loop circuit involving supraspinal structures that, in turn, project top-down to the spinal cord. For this reason, the sP22 encompasses spinal segments rostral and caudal to those where the sP9 and sP13 are recorded (Fig 3 and S1, S2 and S3 Videos).

https://doi.org/10.1371/journal.pbio.3003116.g007

Several pieces of evidence indicate that our sP22 corresponds to the top-down driven P2s of the animal invasive literature: first, its relatively long latency is compatible with the top-down hypothesis arising from animal experiments (Fig 2). Second, the sP22 is the only spinal component that was clearly modulated by our cognitive task (Fig 6). Interestingly, the spatial resolution offered by high-density ESI, allowed us to observe that the sP22 encompasses spinal segments both rostral and caudal to those where the sP9 and sP13 are located (Fig 3). This suggests that sP22 is not a direct consequence of the incoming somatosensory signals—since these would be expected to become evident more rostrally than caudally. Instead, sP22 may reflect stimulus-triggered activation of top-down supraspinal projections (Fig 7). Indeed, only afferents belonging to small-myelinated Aδ and unmyelinated C units travel both rostrally and caudally in the Lissauer's tract after entering the dorsal root, and thus elicit responses [46] and perceptual effects [47] not strictly localized at the level of the dermatomal stimulation. Crucially, these afferents are not activated by the electrical stimulation we used, which preferentially activates large-myelinated, fast-conducting Aβ fibers that project rostrally rather than caudally. Further, the afferent volley from slower fibers does not reach the spinal cord until 35–45 ms after the electrical stimulation. Thus, the combination of the temporal (22 ms latency) and spatial (similar rostral and caudal distribution) properties of the sP22, suggesting a polysynaptic generation mechanism, points towards a supraspinal rather than an afferent origin.

Response lateralization

Consistent with findings reported in the literature, we observed significant evidence of response lateralization at both the Erb's point and the scalp [48]. At the brachial plexus, the eP8 and eN9 responses were detected only on the side ipsilateral to the stimulation, whereas at the scalp, the cN20 and cP25 responses appeared exclusively contralateral to the stimulation (Fig 5).

Previous studies using both invasive recordings in non-human primates and intraoperative monitoring of SEPs in humans have reported the possibility of lateralized spinal responses following median nerve stimulation. More specifically, in anesthetized cynomolgus monkeys, the origin of the negative components comparable to the human sN13 is in the laminae IV-VI of the dorsal horn ipsilateral to the stimulation side [34]. We therefore took advantage of the topographical

information provided by ESI to test whether the responses we recorded were similarly lateralized. To the best of our knowledge, we are the first to perform a point-by-point comparison between right and left stimulation across the full time-course of the stimulus-evoked response. The advantage of performing paired t-tests along the whole time course allows for the identification of effects outside of the temporal regions of interest, such as before or after the peaks of the components. We found no statistical evidence of lateralization at any point during the evoked response (Fig 5). We cannot exclude the possibility that the neural response may in fact be lateralized, but that factors such as the small distance between neighboring electrodes along the mediolateral axis, volume conduction effects, and the low signal-to-noise ratio prevented our recordings from providing reliable evidence of lateralization. Future technical developments, such as reducing electrode size in combination with improved volume conduction models, may enable a more precise spatial definition of the neural sources of the spinal components described here.

Attentional modulation

Cortical top-down control appears to be a general principle of neural organization [49,50]. Such processes may strongly affect neural activity in subcortical structures, including the spinal cord [e.g., 51].

For example, functional MRI studies of the spinal cord have shown that nocebo manipulations enhance pain-related BOLD activity in the dorsal horn ipsilateral to a nociceptive stimulus. This suggests a tonic top-down pain-facilitation mechanism occurring at spinal cord level [52]. Similarly, nociceptive stimuli delivered during high-load cognitive tasks result in lower pain ratings and weaker BOLD responses in the ipsilateral dorsal horn, compared to a low-load control condition [53,54].

However, given that BOLD activity integrates neural activity across several seconds [55], fMRI cannot unravel the temporal dynamics of these modulations. By combining an attentional paradigm with the high temporal resolution of ESI, we were able to show that attention selectively influences specific components of the spinal response (Fig 6). Specifically, we found that the sP22 amplitude (which, as discussed above, is the human equivalent of the P2s recorded in animals and likely reflects stimulus-triggered activation of top-down supraspinal projections) depends strongly on current cognitive task and focus of attention, while earlier spinal and cortical responses do not. This pattern is consistent with recent spinal fMRI findings by Oliva and colleagues [53], who reported higher activity in a dorsal horn cluster during attentional analgesia with noxious thermal stimulation. Although the BOLD signal lacks the temporal precision to disentangle component-specific dynamics, their results converge with our observation of larger sP22 amplitudes when attention was directed away from the somatosensory input [53]. These results are informative about the underlying nature of the attentional modulation that can only be coarsely measured with spinal fMRI. In particular, our results suggest that attention does not cause a *general* gating of all somatosensory-evoked activity at spinal cord level. Instead, attentional effects may be specifically linked to supraspinal modulation of synaptic activity within the spinal cord.

It is important to note that the comparison between the working memory and omission counting tasks was based on a relatively small sample ($N = 13$). While this analysis illustrates that ESI can capture task-related modulation of spinal responses, the limited sample size implies that only relatively large effect sizes are likely to be detected reliably. Future studies should therefore include larger samples to enable the reliable detection of smaller modulatory effects and to better characterize their variability across individuals.

Comparison with other recent noninvasive spinal recording approaches

Recent studies have adopted alternative strategies to attempt noninvasive spinal cord electrophysiology. As we already noted in the Introduction, Nierula and colleagues [13] used a multivariate template-matching approach (CCA), which improved signal-to-noise ratio and even enabled single-trial estimates. In contrast, our ESI approach relies on a deliberately simple, data-driven pipeline that avoids template-based spatial filtering. Although more conservative, our strategy reduces the risk of introducing spurious components and ensures that the signals we describe (sP9, sN13, sP22) are

physiologically interpretable. A potential limitation of the CCA approach is that it is constrained to the predefined response interval on which the template is imposed, and therefore may be less sensitive to activity falling outside that temporal window.

Stenner and colleagues [56] focused instead on high-frequency (~600 Hz) activity as a marker of neuronal output, employing a circular montage of 24 electrodes around the neck. In contrast, our montage of 63 dorsal electrodes was designed to optimize the detection of ascending afferent volleys and postsynaptic spinal components, and, crucially, to reconstruct dynamic images of neural activity unfolding over time (see S1, S2 and S3 Videos). It is worth noting that neither mapping on a cylindrical surface (as in Stenner and colleagues, 2025) nor on a flat surface (as in our technique) is ideal for calculating a neutral reference, where the sum of voltages across all electrodes should equal zero—a condition that is not achieved in either case. However, the flat montage has the important advantage of being more easily converted into a series of bipolar derivations, whereas the cylindrical arrangement poses significant difficulties for such calculations. Thus, although both approaches are suboptimal, a flat montage is influenced by fewer variables and is less susceptible to noise. A final advantage of our montage and analysis approach is that it yields maps of components tightly aligned with established physiological models of spinal processing. The statistical time–frequency maps reported by Stenner and colleagues (e.g., their Fig 2B) are less straightforward to interpret physiologically, as significant clusters do not clearly overlap with defined time–frequency responses and may partly reflect edge effects.

Taken together, these methodological differences highlight how the three approaches (the template-matching of [13], the high-frequency analyses of Stenner and colleagues [56], and our conservative, data-driven ESI) jointly advance the development of noninvasive methods to study human spinal cord activity.

Promise of this technique for pain research

All spinal activities we described were elicited by afferent volleys conducted along non-nociceptive, large-myelinated Aβ tactile afferents. Extending this approach to measure spinal responses to Aδ and C thermal-nociceptive afferents would be particularly relevant. Indeed, enhanced sensitivity of spinal neurons underlies many chronic pain conditions, and effective pain management demands a better understanding of the electrophysiological changes occurring at spinal level [57].

However, recording segmental spinal activity poses tougher challenges than detecting scalp responses. The ascending nociceptive volley is amplified by multiple relays in the central nervous system, producing large and distributed generators that are easier to detect (for a detailed discussion, see [58]). In contrast, spinal recordings reflect smaller, earlier generators with less population summation, leading to a poorer signal-to-noise ratio at the skin over the spine. For these reasons, both stimulus specificity and the activation of as many target fibers as possible are critical. Thermal stimuli, such as radiant laser or contact heat, not only recruit markedly fewer afferents than those engaged by transcutaneous electrical nerve stimulation, but have slow and variable receptor activation, introducing response jitter that can exceed the conduction time of the afferent volley (e.g., Iannetti and colleagues [59]).

Electrical stimulation provides a transient and reliable afferent activity, but selectively exciting nociceptors without recruiting Aβ fibers is technically demanding. Traditional concentric electrodes [60 ,61] have only a narrow selectivity window, because as intensity increases, the deeper fields recruit non-nociceptive fibers, and the effective active area is limited to the cathode point [62].

To overcome these limitations, one of the authors developed the IDE-150 (interdigitated electrode, 150 μm spacing), a comb-like micropatterned device that concentrates current in the superficial epidermis across a broad area, while minimizing deeper spread. Its efficacy has been demonstrated in experimental studies [63 ,64]. For these reasons, we consider spinal nociceptive evoked-potential recordings using the IDE-150 electrode highly promising.

An entirely alternative approach is to use tonic nociceptive stimulation, such as the cold pressure test [65]. In this case, precise timing of stimulus onset is less critical, and postsynaptic spinal activity would more likely be reflected in the time-frequency domain.

Regardless of the specifics of the approach used, the possibility of recording nociceptive spinal cord activity noninvasively holds promise for cost-efficient early diagnosis and stratification of chronic pain patients. Importantly, our present demonstration that top-down modulation of spinal circuits can be detected with ESI (e.g., Fig 6) highlights the potential of this technique to study descending pain control, one of the key mechanisms through which placebo analgesia is thought to act [66; although see 67].

Supporting information

S1 Video. ESI experimental setup and responses.
(MP4)

S2 Video. ESI experimental setup and responses (detail).
(MP4)

S3 Video. sP9 wave traveling.
(MP4)

Acknowledgments

The authors are grateful to all lab members and especially to Drs Cédric Lenoir and Paul Summers for their feedback provided in earlier stages of this work, and to Michele Motta, who generously helped with the collection of additional data. We thank the Data Science and Computation Facility and its Support Team for their assistance on the IIT High Performance Computing Infrastructure.

Author contributions

Conceptualization: Giulio Gabrieli, Gian Domenico Iannetti.

Data curation: Giulio Gabrieli.

Formal analysis: Giulio Gabrieli, Massimo Leandri.

Funding acquisition: Gian Domenico Iannetti.

Investigation: Giulio Gabrieli, Massimo Leandri, Gian Domenico Iannetti.

Methodology: Giulio Gabrieli, Massimo Leandri, Patrick Haggard, Gian Domenico Iannetti.

Project administration: Gian Domenico Iannetti.

Resources: Gian Domenico Iannetti.

Software: Giulio Gabrieli.

Supervision: Gian Domenico Iannetti.

Validation: Giulio Gabrieli, Richard Somervail, André Mouraux, Massimo Leandri, Patrick Haggard, Gian Domenico Iannetti.

Visualization: Giulio Gabrieli, André Mouraux, Massimo Leandri, Patrick Haggard, Gian Domenico Iannetti.

Writing – original draft: Giulio Gabrieli, André Mouraux, Massimo Leandri, Patrick Haggard, Gian Domenico Iannetti.

Writing – review & editing: Giulio Gabrieli, Richard Somervail, André Mouraux, Massimo Leandri, Patrick Haggard, Gian Domenico Iannetti.

References

1. Carter JL, Stevens JC. Somatosensory evoked potentials. In: Clinical neurophysiology. 2009. p. 257–80.
2. Mountcastle VB. The sensory hand: neural mechanisms of somatic sensation. Harvard University Press; 2005.

3. Eisen AA. Noninvasive measurement of spinal cord conduction: review of presently available methods. Muscle Nerve. 1986;9(2):95–103. https://doi.org/10.1002/mus.880090202 PMID: 3513008
4. Eippert F, Kong Y, Jenkinson M, Tracey I, Brooks JCW. Denoising spinal cord fMRI data: approaches to acquisition and analysis. Neuroimage. 2017;154:255–66. https://doi.org/10.1016/j.neuroimage.2016.09.065 PMID: 27693613
5. Giove F, Garreffa G, Giulietti G, Mangia S, Colonnese C, Maraviglia B. Issues about the fMRI of the human spinal cord. Magn Reson Imaging. 2004;22(10):1505–16. https://doi.org/10.1016/j.mri.2004.10.015 PMID: 15707800
6. Maieron M, Iannetti GD, Bodurka J, Tracey I, Bandettini PA, Porro CA. Functional responses in the human spinal cord during willed motor actions: evidence for side- and rate-dependent activity. J Neurosci. 2007;27(15):4182–90. https://doi.org/10.1523/JNEUROSCI.3910-06.2007 PMID: 17428996
7. Logothetis NK. The underpinnings of the BOLD functional magnetic resonance imaging signal. J Neurosci. 2003;23(10):3963–71. https://doi.org/10.1523/jneurosci.23-10-03963.2003
8. Stroman PW. Magnetic resonance imaging of neuronal function in the spinal cord: spinal FMRI. Clin Med Res. 2005;3(3):146–56. https://doi.org/10.3121/cmr.3.3.146 PMID: 16160069
9. Willis WD Jr, Coggeshall RE. Sensory mechanisms of the spinal cord. Springer US; 2004. https://doi.org/10.1007/978-1-4615-0035-3
10. da Silva FL. EEG: origin and measurement. In: Mulert C, Lemieux L, editors. EEG - fMRI: physiological basis, technique, and applications. Springer International Publishing; 2022. p. 23–48. https://doi.org/10.1007/978-3-031-07121-8_2
11. Ertekin C. Comparison of the human evoked electrospinogram recorded from the intrathecal, epidural and cutaneous levels. Electroencephalogr Clin Neurophysiol. 1978;44(6):683–90. https://doi.org/10.1016/0013-4694(78)90202-x PMID: 78796
12. Chander BS, Deliano M, Azañón E, Büntjen L, Stenner M-P. Non-invasive recording of high-frequency signals from the human spinal cord. Neuroimage. 2022;253:119050. https://doi.org/10.1016/j.neuroimage.2022.119050 PMID: 35276364
13. Nierula B, Stephani T, Bailey E, Kaptan M, Pohle L-MG, Horn U, et al. A multichannel electrophysiological approach to noninvasively and precisely record human spinal cord activity. PLoS Biol. 2024;22(10):e3002828. https://doi.org/10.1371/journal.pbio.3002828
14. Hu L, Iannetti GD. Painful issues in pain prediction. Trends Neurosci. 2016;39(4):212–20. https://doi.org/10.1016/j.tins.2016.01.004 PMID: 26898163
15. Li R, Principe JC, Bradley M, Ferrari V. A spatiotemporal filtering methodology for single-trial ERP component estimation. IEEE Trans Biomed Eng. 2009;56(1):83–92. https://doi.org/10.1109/TBME.2008.2002153 PMID: 19224722
16. Mayhew SD, Iannetti GD, Woolrich MW, Wise RG. Automated single-trial measurement of amplitude and latency of laser-evoked potentials (LEPs) using multiple linear regression. Clin Neurophysiol. 2006;117(6):1331–44. https://doi.org/10.1016/j.clinph.2006.02.017 PMID: 16644270
17. Woody CD. Characterization of an adaptive filter for the analysis of variable latency neuroelectric signals. Med Biol Eng. 1967;5(6):539–54. https://doi.org/10.1007/bf02474247
18. Gramfort A, Luessi M, Larson E, Engemann DA, Strohmeier D, Brodbeck C, et al. MEG and EEG data analysis with MNE-Python. Front Neurosci. 2013;7:267. https://doi.org/10.3389/fnins.2013.00267 PMID: 24431986
19. Harris CR, Millman KJ, van der Walt SJ, Gommers R, Virtanen P, Cournapeau D, et al. Array programming with NumPy. Nature. 2020;585(7825):357–62. https://doi.org/10.1038/s41586-020-2649-2 PMID: 32939066
20. Virtanen P, Gommers R, Oliphant TE, Haberland M, Reddy T, Cournapeau D, et al. SciPy 1.0: fundamental algorithms for scientific computing in Python. Nat Methods. 2020;17(3):261–72. https://doi.org/10.1038/s41592-019-0686-2 PMID: 32015543
21. Desmedt JE, Cheron G. Spinal and far-field components of human somatosensory evoked potentials to posterior tibial nerve stimulation analysed with oesophageal derivations and non-cephalic reference recording. Electroencephalogr Clin Neurophysiol. 1983;56(6):635–51. https://doi.org/10.1016/0013-4694(83)90031-7 PMID: 6197282
22. Kaji R, Sumner AJ. Bipolar recording of short-latency somatosensory evoked potentials after median nerve stimulation. Neurology. 1987;37(3):410–8. https://doi.org/10.1212/wnl.37.3.410 PMID: 3822134
23. Lehmkuhl D, Dimitrijevic MR, Renouf F. Electrophysiological characteristics of lumbosacral evoked potentials in patients with established spinal cord injury. Electroencephalogr Clin Neurophysiol. 1984;59(2):142–55. https://doi.org/10.1016/0168-5597(84)90030-3 PMID: 6200308
24. Chabot R, York DH, Watts C, Waugh WA. Somatosensory evoked potentials evaluated in normal subjects and spinal cord-injured patients. J Neurosurg. 1985;63(4):544–51. https://doi.org/10.3171/jns.1985.63.4.0544 PMID: 4032019
25. Hu L, Cai MM, Xiao P, Luo F, Iannetti GD. Human brain responses to concomitant stimulation of Aδ and C nociceptors. J Neurosci. 2014;34(34):11439–51. https://doi.org/10.1523/JNEUROSCI.1355-14.2014 PMID: 25143623
26. Mancini F, Beaumont A-L, Hu L, Haggard P, Iannetti GDD. Touch inhibits subcortical and cortical nociceptive responses. Pain. 2015;156(10):1936–44. https://doi.org/10.1097/j.pain.0000000000000253 PMID: 26058037
27. Massimini M, Huber R, Ferrarelli F, Hill S, Tononi G. The sleep slow oscillation as a traveling wave. J Neurosci. 2004;24(31):6862–70. https://doi.org/10.1523/JNEUROSCI.1318-04.2004 PMID: 15295020
28. Nuwer MR, Aminoff M, Desmedt J, Eisen AA, Goodin D, Matsuoka S, et al. IFCN recommended standards for short latency somatosensory evoked potentials. Report of an IFCN committee. Electroencephalogr Clin Neurophysiol. 1994 Jul;91(1):6–11. https://doi.org/10.1016/0013-4694(94)90012-4 PMID: 7517845

29. Buchthal F, Rosenfalck A. Evoked action potentials and conduction velocity in human sensory nerves. Brain Res. 1966;3(1):v–122. https://doi.org/10.1016/0006-8993(66)90056-4
30. Lorente dNR. A study of nerve physiology. In: Studies from the Rockefeller Institute for Medical Research, vol. 132. Reprints. Rockefeller Institute for Medical Research; 1947. p. 1–548.
31. Jewett DL, Deupree DL. Far-field potentials recorded from action potentials and from a tripole in a hemicylindrical volume. Electroencephalogr Clin Neurophysiol. 1989;72(5):439–49. https://doi.org/10.1016/0013-4694(89)90049-7 PMID: 2469568
32. Dimitrijevic MR, Halter JA. Atlas of human spinal cord evoked potentials. Elsevier Health Sciences; 1995.
33. Campbell B. The distribution of potential fields within the spinal cord. Anat Rec. 1945;91(1):77–88. https://doi.org/10.1002/ar.1090910110
34. Beall JE, Applebaum AE, Foreman RD, Willis WD. Spinal cord potentials evoked by cutaneous afferents in the monkey. J Neurophysiol. 1977;40(2):199–211. https://doi.org/10.1152/jn.1977.40.2.199
35. Bernhard CG, Widén L. On the origin of the negative and positive spinal cord potentials evoked by stimulation of low threshold cutaneous fibres. Acta Physiol Scandinavica. 1953;29(S106):42–54. https://doi.org/10.1111/j.1365-201x.1953.tb10768.x
36. Coombs JS, Curtis DR, Landgren S. Spinal cord potentials generated by impulses in muscle and cutaneous afferent fibres. J Neurophysiol. 1956;19(5):452–67. https://doi.org/10.1152/jn.1956.19.5.452 PMID: 13367876
37. Fernandez de molina A, Gray JA. Activity in the dorsal spinal grey matter after stimulation of cutaneous nerves. J Physiol. 1957;137(1):126–40. https://doi.org/10.1113/jphysiol.1957.sp005801 PMID: 13439589
38. Eccles JC, Sherrington CS. Reflex summation in the ipsilateral spinal flexion reflex. J Physiol. 1930;69(1):1–28. https://doi.org/10.1113/jphysiol.1930.sp002630 PMID: 16994083
39. Gasser HS, Graham HT. Potentials produced in the spinal cord by stimulation of dorsal roots. Am J Physiol Legacy Cont. 1933;103(2):303–20. https://doi.org/10.1152/ajplegacy.1933.103.2.303
40. Willis WD, Weir MA, Skinner RD, Bryan RN. Differential distribution of spinal cord field potentials. Exp Brain Res. 1973;17(2):169–76. https://doi.org/10.1007/BF00235026 PMID: 4714523
41. Jeanmonod D, Sindou M, Mauguière F. The human cervical and lumbo-sacral evoked electrospinogram. Data from intra-operative spinal cord surface recordings. Electroencephalogr Clin Neurophysiol. 1991;80(6):477–89. https://doi.org/10.1016/0168-5597(91)90129-l PMID: 1720723
42. Bernhard CG, Widén L. On the origin of the negative and positive spinal cord potentials evoked by stimulation of low threshold cutaneous fibres. Acta Physiol Scandinavica. 1953;29(S106):42–54. https://doi.org/10.1111/j.1365-201x.1953.tb10768.x
43. Carpenter D, Lundberg A, Norrsell U. Primary afferent depolarization evoked from the sensorimotor cortex. Acta Physiol Scand. 1963;59:126–42. https://doi.org/10.1111/j.1748-1716.1963.tb02729.x PMID: 14065844
44. Shimoji K, Kano T. Evoked electrospinogram: interpretation of origin and effects of anesthetics. Int Anesthesiol Clin. 1975;13(1):171–89. PMID: 1126754
45. Tang AH. Dorsal root potentials in the chloralose-anesthetized cat. Exp Neurol. 1969;25(3):393–400. https://doi.org/10.1016/0014-4886(69)90133-2 PMID: 5351343
46. Porro CA, Cavazzuti M. Functional correlates of acute prolonged pain in the rat central nervous system: 2-DG studies. In: Gonzalez-Lima F, Finkenstädt Th, Scheich H, editors. Advances in metabolic mapping techniques for brain imaging of behavioral and learning functions. Netherlands: Springer; 1992. p. 319–42. https://doi.org/10.1007/978-94-011-2712-7_12
47. Mitchell AG, Ehmsen JF, Christensen DE, Stuckert AV, Haggard P, Fardo F. Disentangling the spinal mechanisms of illusory heat and burning sensations in the thermal grill illusion. Pain. 2024;165(10):2370–8. https://doi.org/10.1097/j.pain.0000000000003352 PMID: 39185673
48. Nuwer MR, Packwood JW. Somatosensory evoked potential monitoring with scalp and cervical recording. In: Handbook of clinical neurophysiology, vol. 8. Elsevier; 2008. p. 180–9. https://doi.org/10.1016/S1567-4231(07)08011-2
49. Colloca L, Barsky AJ. Placebo and nocebo effects. N Engl J Med. 2020;382(6):554–61. https://doi.org/10.1056/NEJMra1907805 PMID: 32023375
50. Fields H. State-dependent opioid control of pain. Nat Rev Neurosci. 2004;5(7):565–75. https://doi.org/10.1038/nrn1431 PMID: 15208698
51. Seki K, Fetz EE. Gating of sensory input at spinal and cortical levels during preparation and execution of voluntary movement. J Neurosci. 2012;32(3):890–902. https://doi.org/10.1523/JNEUROSCI.4958-11.2012 PMID: 22262887
52. Geuter S, Büchel C. Facilitation of pain in the human spinal cord by nocebo treatment. J Neurosci. 2013;33(34):13784–90. https://doi.org/10.1523/JNEUROSCI.2191-13.2013 PMID: 23966699
53. Oliva V, Hartley-Davies R, Moran R, Pickering AE, Brooks JC. Simultaneous brain, brainstem, and spinal cord pharmacological-fMRI reveals involvement of an endogenous opioid network in attentional analgesia. Elife. 2022;11:e71877. https://doi.org/10.7554/eLife.71877 PMID: 35080494
54. Sprenger C, Eippert F, Finsterbusch J, Bingel U, Rose M, Büchel C. Attention modulates spinal cord responses to pain. Curr Biol. 2012;22(11):1019–22. https://doi.org/10.1016/j.cub.2012.04.006 PMID: 22608507
55. Logothetis NK, Pauls J, Augath M, Trinath T, Oeltermann A. Neurophysiological investigation of the basis of the fMRI signal. Nature. 2001;412(6843):150–7. https://doi.org/10.1038/35084005 PMID: 11449264
56. Stenner MP, Nossa CM, Zaehle T, Azañón E, Heinze HJ, Deliano M, et al. Prior knowledge changes initial sensory processing in the human spinal cord. Sci Adv. 2025 Jan;11(3):eadl5602.

57. Woolf CJ. Central sensitization: implications for the diagnosis and treatment of pain. Pain. 2011;152(3 Suppl):S2–15. https://doi.org/10.1016/j.pain.2010.09.030 PMID: 20961685

58. Somervail R, Perovic S, Bufacchi RJ, Caminiti R, Iannetti GD. A two-system theory of sensory-evoked brain responses. Brain. 2025.

59. Iannetti GD, Leandri M, Truini A, Zambreanu L, Cruccu G, Tracey I. Aδ nociceptor response to laser stimuli: selective effect of stimulus duration on skin temperature, brain potentials and pain perception. Clin Neurophysiol. 2004 Nov;115(11):2629–37. https://doi.org/10.1016/j.clinph.2004.05.023

60. Kaube H, Katsarava Z, Käufer T, Diener HC, Ellrich J. A new method to increase nociception specificity of the human blink reflex. Clin Neurophysiol. 2000 Mar;111(3):413–6. https://doi.org/10.1016/S1388-2457(99)00295-3

61. Inui K, Tran TD, Hoshiyama M, Kakigi R. Preferential stimulation of Aδ fibers by intra-epidermal needle electrode in humans. Pain. 2002 Apr;96(3):247–52. https://doi.org/10.1016/S0304-3959(01)00453-5

62. Mouraux A, Iannetti GD, Plaghki L. Low intensity intra-epidermal electrical stimulation can activate Aδ-nociceptors selectively. Pain. 2010;150(1):199–207. https://doi.org/10.1016/j.pain.2010.04.026 PMID: 20510515

63. Leandri M, Marinelli L, Siri A, Pellegrino L. Micropatterned surface electrode for massive selective stimulation of intraepidermal nociceptive fibres. J Neurosci Methods. 2018 Jan;293:17–26. https://doi.org/10.1016/S0304-3959(01)00453-5

64. Leandri M, Di Stefano G, Truini A, Marinelli L. Early nociceptive evoked potentials (NEPs) recorded from the scalp. Clin Neurophysiol. 2021 Nov;132(11):2896–906. https://doi.org/10.1016/j.clinph.2021.05.027

65. Fanninger S, Plener PL, Fischer MJM, Kothgassner OD, Goreis A. Water temperature during the cold pressor test: a scoping review. Physiol Behav. 2023;271:114354. https://doi.org/10.1016/j.physbeh.2023.114354 PMID: 37717684

66. Eippert F, Finsterbusch J, Bingel U, Büchel C. Direct evidence for spinal cord involvement in placebo analgesia. Science. 2009;326(5951):404. https://doi.org/10.1126/science.1180142 PMID: 19833962

67. Martini M, Lee MCH, Valentini E, Iannetti GD. Intracortical modulation, and not spinal inhibition, mediates placebo analgesia. Eur J Neurosci. 2015;41(4):498–504. https://doi.org/10.1111/ejn.12807 PMID: 25523008